Dynamic Solvation Effects in I^-_2(CO_2)_n Impact onto Solid Surface : Wedge and Cage Effects

Sci. Rep. RITU A41 (1996) pp. 201-205
No. 2, January 1996

Dynamic Solvation Effects in $I_2^-(CO_2)_n$ Impact onto Solid Surface – Wedge and Cage Effects

Hisato Yasumatsu[a], Shin'ichi Koizumi[a,b], Akira Terasaki[a,b] and Tamotsu Kondow[a,b]
[a] *The Institute of Physical and Chemical Research (RIKEN), Wako, Saitama 351-01, Japan*
[b] *Department of Chemistry, School of Science, The University of Tokyo, Bunkyo-ku, Tokyo 113, Japan*

(Received November 14, 1995)

Novel mechanisms were found to operate in dissociation of I_2^- embedded in a CO_2 cluster, $I_2^-(CO_2)_n$, by its impact onto a silicon surface. The bond of I_2^- is split by a CO_2 molecule located halfway between the two iodine atoms in the parent $I_2^-(CO_2)_n$, as if the CO_2 molecule behaves as a molecular 'wedge' (wedge effect). On the other hand, the dissociation of I_2^- is suppressed when it is caged in a complete CO_2 molecular shell (cage effect). The wedge effect was also demonstrated by a molecular-dynamics simulation. By measuring the surface-parallel component of the translational energy of the I_2^- and I^- product anions, it was concluded that a 'quasi-equilibrium' was established on the surface before the product anions leave from it. The translational-energy distribution of the product anions also shows the cage effect.

KEYWORDS: $I_2^-(CO_2)_n$, cluster impact, silicon surface, wedge effect, cage effect, translational-energy distribution, quasi-equilibrium

1. Introduction

Molecular-dynamics-simulation studies by groups of Levine and Jortner [1,2] have clarified that dissociation of I_2 embedded in a rare-gas cluster, $I_2(Rg)_n$ (Rg: rare-gas atom), by its impact on a hard wall ('cluster impact') is greatly assisted by the Rg atom; even chemically-inert Rg atoms participate to the I_2-bond dissociation. Experimentally, we have investigated the dissociation of $I_2^-(CO_2)_n$ in collision with a silicon surface [3-5]. The result shows that dissociation of I_2^- is assisted by the CO_2 molecules, but the degree of the assistance depends markedly on the number, n, of CO_2 molecules present in the cluster anion. The characteristic n-dependence is explained in terms of the structure of $I_2^-(CO_2)_n$; the wedge effect that the CO_2 molecules located halfway between the two iodine atoms assist to split the I_2^- bond as a 'wedge' vs. the cage effect that the CO_2 molecules forming a complete solvation shell around I_2^- reheal the I_2^- dissociation.

These dynamic solvation effects are considered to be operative in the first step of the cluster impact. As the cluster impact induces vigorous many-body collisions among the cluster constituents and surface atoms in the vicinity of the cluster-impact point in several picoseconds, a 'quasi-equilibrium' including the constituents and the surface atoms is accomplished [6,7], in which the internal energy of the quasi-equilibrium might be redistributed, and the 'temperature' of the quasi-equilibrium increases greatly ('cluster-impact heating'): In a computer simulation of Ar_{561} impact onto a NaCl(001) surface, the argon cluster is heated up to ~4000 K [8]. These microscopic dynamics of the cluster impact should be reflected in the amounts and the energy distribution of the products. In the present study, we observed mass spectra of product anions and analyzed their translational energy (surface-parallel component), when a size-selected cluster anion, $I_2^-(CO_2)_n$, was allowed to collide with a silicon surface.

2. Experimental

A tandem time-of-flight (TOF) mass-spectrometer [9] having a cluster-ion source and a surface-collision chamber was used. As a detailed description of the mass spectrometer [9] and the cluster-ion source [3-5] has been reported elsewhere, only a brief description related to the present study is given. Cluster anions, $I_2^-(CO_2)_n$, were produced by injecting 100-350-eV electrons into a supersonic expansion of CO_2 gas containing 1 mol% of I_2 at a stagnation pressure of $1\text{-}2\times10^5$ Pa [10], admitted through a skimmer into an ion-extraction chamber, and accelerated to 4150 eV. A cluster anion, $I_2^-(CO_2)_n$, with a given size, n, was selected out from a train of spatially mass-selected cluster anions with a pulsed deflector (mass gate) placed in the primary TOF mass spectrometer.

Figure 1 shows a schematic diagram of surface-collision and product-detection regions.
A cluster ion, $I_2^-(CO_2)_n$, thus selected was allowed to collide with a silicon surface placed at the bottom of a reflectron at a collision energy per I_2^-, E_{col}, of 1-100 eV under an ambient pressure of $4\text{-}10\times10^{-8}$ Pa. Unless otherwise noted, a collision energy per I_2^- is given. Product anions scattered from the surface were re-accelerated in the same electric field that was used for deceleration of the incoming parent cluster anion, and were mass-analyzed in the secondary TOF mass-spectrometer.

Simultaneously, a surface-parallel component, $E_s^{//}$, of the translational energy of a product anion was determined by changing the ion-detector position in a line almost parallel to the surface as shown in Fig. 1 by arrows. The surface-parallel component, $E_s^{//}$, of the translational energy is related to the detector position as,

$$|E_s^{//}| = (qV_S + E_s^{\perp})\tan^2\phi, \quad (1)$$

where q is an electric charge of the product anions, V_S is a bias voltage applied to the surface, ϕ is an angle between the surface-normal direction and the trajectory of a product anion concerned, and $E_s^{\perp}$ is the surface-normal

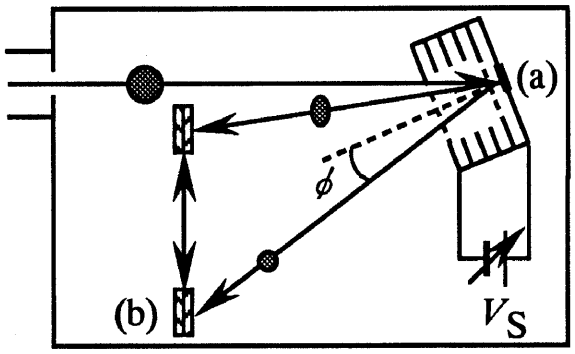

Figure 1. Schematic diagram of surface-collision and product detection regions. The silicon surface (a) is biased with a high-voltage of V_S. Position of the ion detector (b) can be changed almost in parallel to the surface shown as arrows so as to measure a surface-parallel component of the translational energy of the product anions. ϕ is an angle between the surface-normal direction and the trajectory of a product anion concerned.

component of the translational energy of the product anion. The surface-parallel component, $E_s^{\perp}$, was found to be negligible compared with the re-acceleration energy for the product anions. Thus eq. (1) is reduced to

$$|E_s^{//}| \sim qV_S \tan^2 \phi. \quad (2)$$

The silicon surface was prepared by heating a Si(100) wafer (15 mm×25 mm) to 1000 K under an ambient pressure of 3×10^{-7} Pa; the surface is expected to be covered with several amorphous-oxide layers after this heat treatment. The amorphous-oxide layers were intentionally left on the wafer surface in order to suppress electron transfer from $I_2^-(CO_2)_n$ to the surface.

3. Results

When $I_2^-(CO_2)_n$ was admitted to the silicon surface, $I^-(CO_2)_m$ (m=0-2) and $I_2^-(CO_2)_{m'}$ (m'=0-2) were scattered from the surface. The former anions result from recombination of CO_2 with I^- produced by the I_2^- dissociation, while the latter from recombination of CO_2 with I_2^-.

3.1. Dissociation of I_2^- Core Ion

The rate of the I_2^- dissociation can be represented by a branching fraction, f_{dis}, as

$$f_{dis} = \frac{\sum_{m=0}^{2} [I^-(CO_2)_m]}{\sum_{m'=0}^{2} \{[I^-(CO_2)_{m'}] + [I_2^-(CO_2)_{m'}]\}}, \quad (3)$$

where [X] represents an intensity of X, which is obtained by integrating the intensities of the product anions having different $E_s^{//}$. The branching fraction, f_{dis}, increases monotonically and tends to level off with increase in E_{col}. In the $E_{col}\geq$30 eV range, f_{dis} increases by adding CO_2 molecules to I_2^-. This increase implies that the CO_2 molecules contribute to dissociation of I_2^- above the collision energy of 30 eV. Figure 2 shows the dependence of f_{dis} on the parent cluster size, n, at the collision energy of E_{col}=50 eV and at almost normal incident angles (Θ<20 °, where Θ is the incident angle with respect to the surface normal).

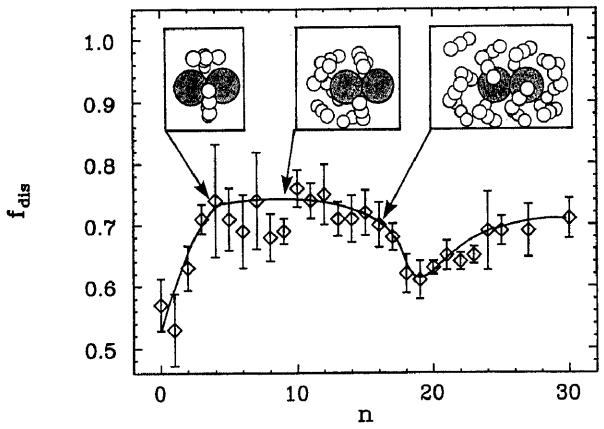

Figure 2. Branching fraction, f_{dis} (see text), of I_2^- dissociation by the impact of $I_2^-(CO_2)_n$ onto a silicon surface is plotted against n at the collision energy (per I_2^-) of 50 eV and at almost normal incident angles (<20 ° with respect to the surface normal). The geometrical structures of $I_2^-(CO_2)_n$ (n=4, 9 and 16) are shown in the insets [11]. The solid curve is shown for an eye-guide.

The uncertainty in f_{dis} originates mainly from a statistical error of the ion intensity of the product anions. For comparison, the key structures of $I_2^-(CO_2)_n$ with n=4, 9, and 16 [11] are shown in the insets of Fig. 2.

3.2. $E_s^{//}$ Distribution of Product Anions

Figure 3 shows the intensities of the product anions plotted against $E_s^{//}$ for the $I_2^-(CO_2)_{16}$ impact at the collision energy of 50 eV and at the incident angle of Θ=26 °, where positive and negative $E_s^{//}$ correspond to ϕ>0 and <0, respectively.

The uncertainties in the ion intensities originate mainly from their statistical error, while those in $E_s^{//}$ mainly from a systematic error in the accuracy of the ion-detector position. The intensities of the product anions were calibrated against the gain of the MCP ion-detector for each product anion [12], but any further instrumental functions were not taken into account for signal calibration. The essential features of the $E_s^{//}$ distribution did not depend on the parent cluster size in the size range studied: (1) All the product anions have almost the same $E_s^{//}$ distribution. (2) The $E_s^{//}$ distributions have a maximum at $E_s^{//}$=0 eV, and is symmetrical with respect to $E_s^{//}$=0 eV. (3) The population of the $E_s^{//}$ distributions decreases exponentially with $|E_s^{//}|$.

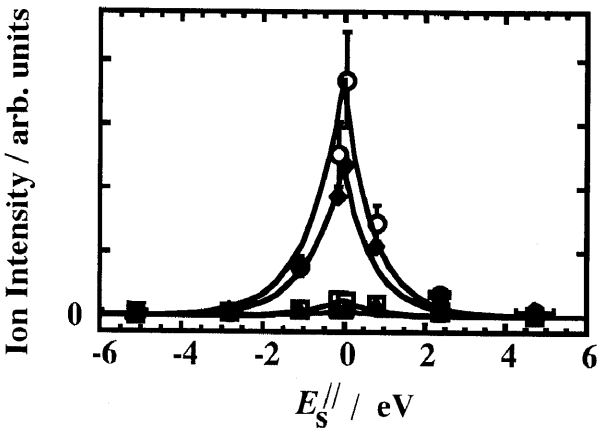

Figure 3. Intensities of the product anions, I^- (○), $I^-(CO_2)$ (□), I_2^- (♦), $I_2^-(CO_2)$ (▲), in $I_2^-(CO_2)_{16}$ impact onto a silicon surface at the collision energy (per I_2^-) of 50 eV and at the incident angle of 26 ° with respect to the surface normal, as a function of the surface-parallel component, $E_s^{//}$, of the translational energy of the product anions. The solid curves are obtained by fitting the experimental $E_s^{//}$ distribution to a one-dimensional Maxwell-Boltzmann distribution having an effective temperature of $T_s^{//}$=8000 K (see text).

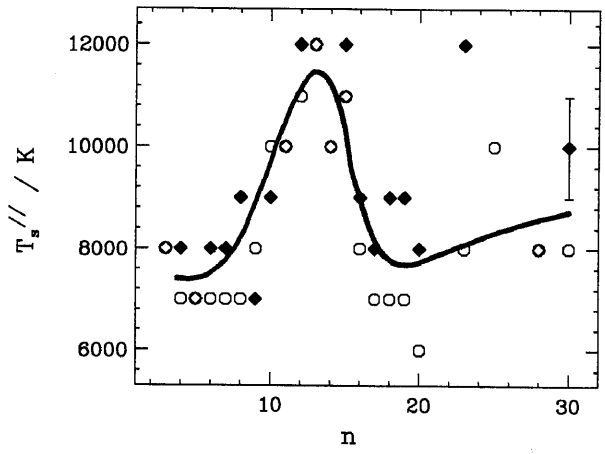

Figure 4. The n-dependence of the effective temperatures, $T_s^{//}$, obtained from the $E_s^{//}$ distribution of the product anions, I^- (○) and I_2^- (♦), for the impact of $I_2^-(CO_2)_{16}$ onto a silicon surface at the collision energy (per I_2^-) of 50 eV and at the incident angle of 26 ° with respect to the surface normal. The solid curve provides an eye guide.

Because of feature (3) stated above, the $E_s^{//}$ distribution was assumed to obey a one-dimensional Maxwell-Boltzmann law having an effective temperature, $T_s^{//}$, as

$$P(v_s^{//})dv_s^{//} \propto \exp\left\{-\frac{m(v_s^{//})^2}{2k_BT_s^{//}}\right\}dv_s^{//} \quad (4)$$

$$= \exp(-\frac{E_s^{//}}{k_BT_s^{//}})dv_s^{//}, \quad (5)$$

where $P(v_s^{//})dv_s^{//}$ is a population of a product anion having a surface-parallel velocity between $v_s^{//}$ and $v_s^{//}+dv_s^{//}$, m is the mass of a product anion, and k_B is the Boltzmann constant. The real $E_s^{//}$ distribution was simulated by taking into account instrumental functions such as divergence of the parent-cluster-anion beam on the surface and a diameter of the MCP ion-detector; the diameter of the parent-cluster-anion beam was measured to be 7 mm with a position-sensitive ion-detector, whereas the effective diameter of the MCP ion-detector was 14 mm. The one-dimensional Maxwell-Boltzmann distribution was convoluted with both the divergence of the parent-cluster-anion beam on the surface and the effective diameter of the ion detector so as to fit the experimental results with a fitting parameter, $T_s^{//}$: As the diameter of the parent-cluster-anion beam is 7 mm, the section of the parent-cluster-anion beam on the surface was mimicked by an elliptic disk having the heights of minor- and major axes of 7 and 7.8(=7/cos 26 °) mm, respectively, where the incident angle of the parent cluster anion is Θ=26 ° with respect to the surface normal. On the other hand, the shape of the ion-detector was approximated by a circle with a diameter of 14 mm. Solid curves in Fig. 3 show the $E_s^{//}$ distributions calculated with $T_s^{//}$=8000 K, where the calculated distributions were normalized with the maximum intensities of the corresponding product anions. The uncertainty in $T_s^{//}$ of ±1000 K originates mainly from ambiguity in the fitting procedure. The best-fit distributions agree well with the experimental ones.

Figure 4 shows the n-dependence of $T_s^{//}$ for the I_2^- and I^- product anions in the $I_2^-(CO_2)_n$ impact at E_{col}=50 eV and Θ=26 °.
The effective temperature, $T_s^{//}$, for the I_2^- product anion is almost the same as that for the I^- product anion. As n increases, both $T_s^{//}$'s increase for $n \leq 12$, decrease for $13 \leq n \leq \sim 18$, and increase again for $n \geq \sim 19$; there is a dip in the $13 \leq n \leq \sim 18$ range.

4. Discussion

4.1. Dissociation of I_2^- Core Ion

The n-dependence of the branching fraction of the I_2^- dissociation (Fig. 2) exhibits (1) a sharp rise in the $0 \leq n \leq 4$ range, (2) almost size-independent f_{dis} in the $5 \leq n \leq 15$ range, and (3) a dip in the vicinity of $n \sim 16$. The comparison of feature (1) with the geometries of $I_2^-(CO_2)_n$ ($0 \leq n \leq 4$) leads us to conclude that a CO_2 molecule located halfway between the two iodine atoms (see the geometry of $I_2^-(CO_2)_4$ in the inset of Fig. 2) splits the I_2^- bond efficiently as if the CO_2 molecule acts as a 'molecular wedge' for the splitting of the I_2^- bond. Feature (3) is attributable to completion of the first solvation shell of the CO_2 molecules at n=16 (cage effect). The decreasing portion of the dip results from an increasing geminate-recombination rate between the

separating I and I^- pair in the solvation shell [10,14,15], while its increasing portion is attributable to an increasing contribution of CO_2 molecular wedges in the second solvation shell to the I_2^- splitting.

A molecular-dynamics simulation lends a further support for the wedge effect. For a demonstration of the wedge effect, collision of I_2^- and $I_2^-(CO_2)$ on a Si(100) surface was simulated. The algorithm used was the fifth-order Gear's predictor-corrector method [16]. These anions were allowed to collide with the Si(100) surface consisting of ~1000 Si atoms at the collision energy of 50 eV, maintaining their I_2^- molecular axes parallel to the surface, where the surface-parallel and normal components of the collision energy were set to be 10 eV and 40 eV, respectively. In the $I_2^-(CO_2)$ impact, the CO_2 molecule was positioned halfway between the two iodine atoms [11] and between I_2^- and the surface. The Si atoms were placed in the sites of the diamond structure with four valences of each Si atom. The potential energy of each collision system was calculated by summing the two-body potentials between all the component species: The potential energy between I_2^- and CO_2 was approximated by Lenard-Jones and electrostatic potentials [11], and that between each component species of the incoming anion and a silicon atom was mimicked by a soft-core potential consisting of a αr^{-9} term, where r is an internuclear distance and α=7 eVÅ^9. The intramolecular potential of I_2^- and those of CO_2 were approximated by a Morse potential [17] and harmonic oscillator potentials, respectively. The potential energy between two silicon atoms was approximated by a Lenard-Jones potential.

Figure 5 shows snapshots of the $I_2^-(CO_2)$ collision event.

The cluster anion, $I_2^-(CO_2)$, positioned at 10 Å apart from the surface at the time, t=0 fs, approaches to the surface and simultaneously CO_2 approaches to I_2^- (t=120 fs). As shown in the picture, CO_2 splits I_2^- into I and I^- at t=210 fs. As the mass of CO_2 is much smaller than that of I, CO_2 is scattered back into vacuum right after the I_2^- splitting as shown in the picture at t=420 fs. These snapshots demonstrated the splitting of the I_2^- bond by the CO_2 molecular wedge. Figure 6 shows time evolution of the I_2^- vibrational energy during the $I_2^-(CO_2)$ collision event.

For comparison, the I_2^- vibrational-energy in the impact of a bare I_2^- is also shown in the figure. Here, the vibrational energy is calculated by summing the potential energy of I_2^- and the relative translational energy between the two iodine atoms along the I_2^- molecular axis. In the $I_2^-(CO_2)$ impact, the vibrational energy increases sharply up to 6 eV at about 100 fs. This increase shows efficient transmission of the CO_2 translational energy to the vibrational degree of freedom of I_2^- (wedge effect). The decrease of the vibrational energy at about 200 fs is caused by vibrational energy dissipation to surface-phonon modes, which induces a shock wave in the surface.

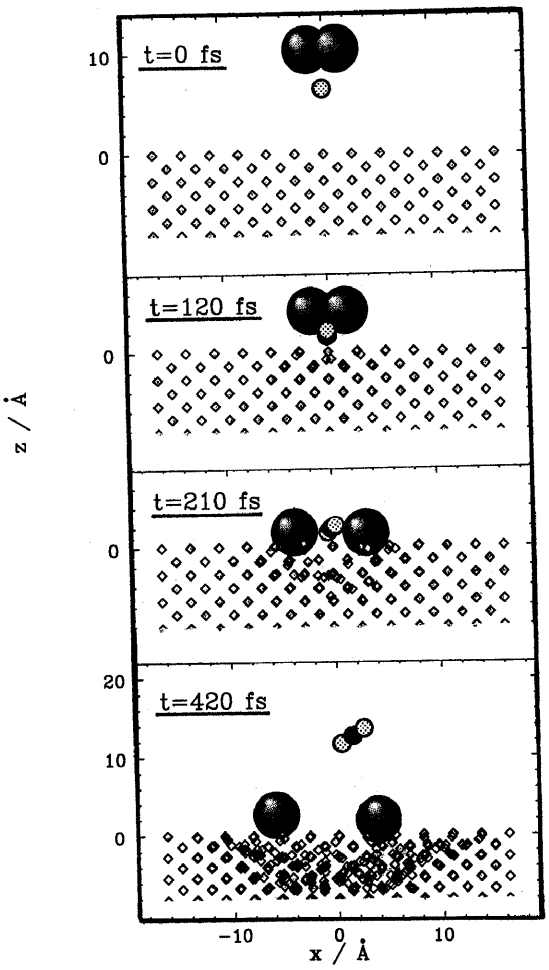

Figure 5. Snapshots of a $I_2^-(CO_2)$ collision event calculated by the molecular-dynamics simulation given in the text. In each shot, the large and the small spheres show iodine atoms and a carbon dioxide molecules, respectively, while diamonds show silicon atoms.

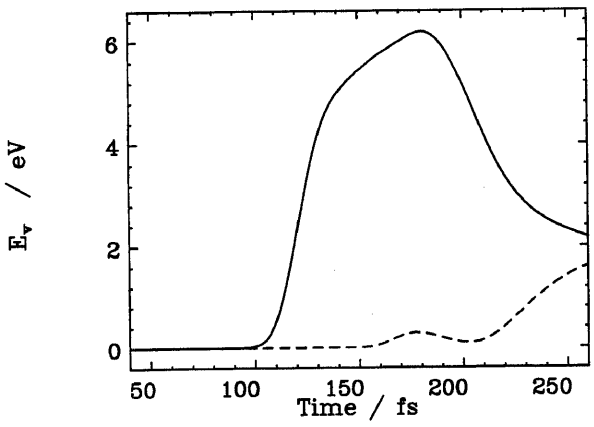

Figure 6. Time evolution of the vibrational energies of I_2^- for I_2^- (dashed curve) and $I_2^-(CO_2)$ (solid curve) collision events. These are calculated by the molecular-dynamics simulation.

4.2. $E_s^{//}$ Distribution

Although the parent cluster anion, $I_2^-(CO_2)_n$, has a surface-parallel component of the collision energy (per I_2^-) as much as 10 eV at E_{col}=50 eV and Θ=26 °, $E_s^{//}$ for the I^- and I_2^- product anions reveals symmetrical distributions with respect to $E_s^{//}$=0 eV, namely, the distributions are isotropic. Thus, in the cluster impact, the constituent species of the parent cluster anion lose their memories that the parent cluster anion had before the impact. In addition, $E_s^{//}$ obeys the one-dimensional Maxwell-Boltzmann distribution having the effective temperature, $T_s^{//}$, which does not depend on the mass of the product anion. These experimental results show that vigorous many-body collisions occur among the constituent species and surface atoms located in the vicinity of the cluster-impact point. The translational energy of the incident cluster anion is redistributed completely among the cluster-constituent species and the surface atoms; a 'quasi-equilibrium'. The n-dependence of $T_s^{//}$ (see Fig. 4) is explained in terms of 'cluster-impact heating' and the cage effect as follows: Large $T_s^{//}$'s imply that the translational energy of a parent cluster anion onto the surface is converted efficiently to its internal energies and hence $T_s^{//}$ specifying the quasi-equilibrium becomes very high (cluster-impact heating). On the other hand, $T_s^{//}$'s should increase with the cluster size, n, since the total energy of the parent cluster anion increases linearly with n, although the collision energy per I_2^- is fixed. The reduction of $T_s^{//}$'s in the $12 \leq n \leq \sim 18$ is ascribable to the formation of the CO_2 cage around the core ion, I_2^- [3-5].

Acknowledgements

We are grateful to Professors R. D. Levine and J. Jortner for their illuminative discussion on the present study. One of the authors, H. Y., is supported by Special Postdoctoral Researchers Program of RIKEN.

1) I. Schek, T. Raz, R. D. Levine and J. Jortner, J. Chem. Phys. **101** (1994) 8596.
2) T. Raz, I. Schek, M. Ben-Num, U. Even, J. Jortner and R. D. Levine, J. Chem. Phys. **101** (1994) 8606.
3) H. Yasumatsu, A. Terasaki and T. Kondow, Submitted to Science (1995).
4) H. Yasumatsu, U. Kalmbach, A. Terasaki and T. Kondow, Proceedings of Yamada Conference XLIII on Structures and Dynamics of Clusters, In press (1996).
5) H. Yasumatsu, T. Tsukuda, T. Sugai, A. Terasaki, T. Nagata and T. Kondow, Surf. Rev. Lett. In press (1995).
6) H. Vach, M. Benslimane, M. Châtelet, A. D. Martino, F. Pradère, J. Chem. Phys. **103**, 1972 (1995).
7) M. Benslimane, M. Châtelet, A. D. Martino, F. Pradère and H. Vach, Chem. Phys. Lett. **273** (1995) 323.
8) C. L. Cleveland and U. Landman, Science **257** (1992) 335.
9) T. Tsukuda, H. Yasumatsu, T. Sugai, A. Terasaki, T. Nagata and T. Kondow, J. Phys. Chem. **99** (1995) 6367.
10) J. M. Papanikolas, J. R. Gord, N. E. Levinger, D. Ray, V. Vorsa and W. C. Lineberger, J. Phys. Chem. **95** (1991) 8028.
11) F. G. Amar and L. Perera, Z. Phys. D**20** (1991) 173.
12) The gain of the micro-channel-plate ion-detector used in the present study was assumed to be proportional to a velocity of ions detected [13].
13) E. A. Kunz, Am. Lab. **11** (1979) 67.
14) J. M. Papanikolas, P. E. Maslen and R. Parson, J. Chem. Phys. **102** (1995) 2452.
15) J. M. Papanikolas, V. Vorsa, M. E. Nadel, P. J. Campagnola, H. K. Buchenau and W. C. Lineberger, J. Chem. Phys. **93** (1993) 8733.
16) M. P. Allen and D. J. Tildesley, Computer Simulations of Liquids (Clarendon Press, Oxford, 1987).
17) E. C. M. Chen and W. E. Wentworth, J. Phys. Chem. **89** (1985) 4099.